Microchimica Acta (2020) 187:360
https://doi.org/10.1007/s00604-020-04348-x

ORIGINAL PAPER

An aptasensor strip-based colorimetric determination method for kanamycin using cellulose acetate nanofibers decorated DNA–gold nanoparticle bioconjugates

Mohammed Awad Abedalwafa[1,2] · Zhimin Tang[1] · Yansha Qiao[1] · Qianqian Mei[1] · Gang Yang[1] · Yan Li[1] · Lu Wang[1]

Received: 21 September 2019 / Accepted: 18 May 2020

Abstract

The preparation of portable colorimetric biosensor strips is described by combining aptamer-immobilized electrospun nanofiber membranes (A-NFMs) with signal probes (DNA-conjugated gold nanoparticles (AuNPs)) for determination of kanamycin (KMC) as a model analyte. The A-NFMs were decorated with complementary single-stranded DNA (cDNA) of KMC aptamer-conjugated AuNPs (cDNA@Au) to get the colorimetric biosensor strips. The constructed biosensor strips showed a significant absorbance decreasing band at 510 nm which induce a visual color change from pink to white when exposed to KMC, with a low detection limit of 2.5 nM (at $S/N = 3$). The effect is due to disassembling of cDNA@Au from NFMs in the presence of KMC because the aptamer has a higher affinity to KMC than its complementary DNA, which resulted in replacing cDNA@Au with KMC. Satisfactory performance was observed in real sample (drinking water and milk) analysis with a recovery of 98.9–102.2%. The constructed colorimetric biosensor test strips hold great application promise for food safety control.

Keywords Aptamer · Electrospun nanofiber membrane · Antibiotic residue · Signal probes · Colorimetric assay

Introduction

A global rise in new diseases is emerging coupled with the increase of antimicrobial resistance which threaten humanity's booming population, and it is responsible for 33,000 annual deaths in Europe alone [1, 2]. By the year 2050, the antibiotic resistant superbugs will be surpassing cancer as the leading cause of mortality worldwide [3, 4]. One of the factors that has led to this crisis is the antibiotics abuse in livestock breeding [5]. Therefore, advancements in antibiotic residue determination have gained considerable traction as a food safety measure. To detect antibiotics residual in animal-derived food, various methods, such as gas chromatography-mass spectrometry [6, 7], high-performance liquid chromatography (HPLC) [8], and high-performance liquid chromatography-tandem mass spectrometry [9], are conducted. These methods present high reliability, sensitivity, and selectivity; however, they also require for expensive equipment and trained operators [10, 11]. Thus, it is highly demanded to promote inexpensive, rapid, and accurate methods.

Common people always prefer tools that have cleared test process, easy-used procedure, and intuitionistic readout; therefore, point-of-care testing (POCT) methods have an unparalleled attraction in monitoring antibiotic residues in food samples [12]. As one of the most popular POCT methods, enzyme-linked immunosorbent assay (ELISA) kit is a user-friendly method, but it still suffers the intrinsic limitation of expensive antibody, and requires harsh preservation condition and batch-to-batch variations of quality [13]. Despite desirable progress have been achieved, there is still an urgent demand to explore stable methods for the quick screening of antibiotics

Electronic supplementary material The online version of this article (https://doi.org/10.1007/s00604-020-04348-x) contains supplementary material, which is available to authorized users.

✉ Yan Li
yanli@dhu.edu.cn

✉ Lu Wang
wanglu@dhu.edu.cn

[1] Key Laboratory of Textile Science & Technology, Ministry of Education, College of Textiles, Donghua University, Shanghai 201620, China

[2] Department of Technical Textile, Faculty of Industries Engineering & Technology, University of Gezira, 21111 Wad Madani, Sudan

Published online: 29 May 2020

in food. Another issue may result from the shortage of proper carrier materials to instead of nitrocellulose filter papers for recognition ligands decorating [14]. In comparison with antibodies, aptamers, single-stranded DNA oligomers, have great advantages for small molecule determination. When the molecular weight of molecules is smaller than 2000 g mol^{-1}, specific antibody is usually hard to generate due to insufficient immunogenicity, but the small molecule aptamers possess great affinity and specificity to the target [15]. Consequently, aptasensor methods have been developed for antibiotic residues determination using different electrochemical [16], microchip electrophoresis [17], fluorescent [18, 19], and colorimetric schemes [20]. Out of these, colorimetric aptasensor has several advantages owing to their capacity to carry out fast and low-cost portability and simplicity [21]. Up to now, almost all of the existing colorimetric aptasensors are colloid-based assays, which is created by controlling the assembly and disassembly of gold nanoparticle (AuNP) colloid aptamer conjugates [22, 23]. However, aptasensor strips have never been developed due to the limited availability of suitable carrier materials.

Over the last years, it has been demonstrated that introducing electrospun nanofibrous membranes (NFMs) as the platform for recognition element functionalization can sustainably improve sensitivity and portability [24, 25]. Electrospinning is a simple but powerful technique, which can help fabricate NFMs with self-standing structure, high specific surface area (SSA), and porosity, and easy to functionalize. Additionally, with interrelated tortuous porous structures, the analyte diffusion can facilitate and accelerate the interaction between analyte and recognition sites [26]. Hence, it can be employed to label aptamer as probes and fabricate test strips for the determination of antibiotics. So far, studies on NFM-based antibiotics colorimetric sensors have not been available. Moreover, the crux of the matter is that the Au and aptamer are investigated separately, only focus on AuNPs decorated NFMs for photocatalysis [27], or aptamer-immobilized NFMs for electrochemical recognizing [28]. Researchers before have never systematically addressed the significance of integrating aptamer-AuNPs bioconjugates with NFMs together for colorimetric sensing.

Considering the above findings, a stable and portable colorimetric strip was constructed for detecting kanamycin (KMC) as a model analyte. In particular, a nanofibrous carrier with carboxyl groups was fabricated by grafting glutamic acid (GA) into cellulose acetate (CA) (G-CA NFMs). In this assay, a KMC aptamer was first labeled on G-CA NFMs. Secondly, the signal probes consisting of a complementary single-stranded DNA (cDNA) of KMC aptamer-conjugated AuNPs were hybridized with aptamer on G-CA NFMs. In the presence of KMC, because the aptamer presents higher affinity to the target than to its complementary DNA, the KMC can replace the cDNA then the signal probes would disassembly from G-CA NFMs finally. These test strips were successfully employed to detect KMC residues in food samples. All results prove that our biosensor strips can be widely applied for fast, sensitive, and portable recognition of KMC in real samples.

Experimental

Materials and reagents

All chemicals were utilized as received without any further purification and acquired from sources. Hydrogen tetrachloroaurate (III), acetone, N, N-dimethylacetamide (DMAc), sodium hydroxide (NaOH), hydrochloric acid (HCl), sodium chloride (NaCl), trisodium citrate, nitric acid (HNO3), N-hydroxysuccinimde (NHS), 1-ethyl-3-(3-(dimethylamino)propyl) carbodiimide (EDC), CA (39.8 wt%, Mw = 30,000), and GA were procured from Shanghai Aladdin Biochemical Technology Co., Ltd. (http://www.aladdin-e.com). Phosphate-buffered saline (PBS, 0.2 M, pH 7.4) (raising to pH 8.0 by adding KOH) and 2-(N-morpholino) ethanesulfonic acid (MES, 50 mM, pH = 5.5) were gained from Quality Life Technologies Co., Ltd. (http://www.cnqlt.com). All the antibiotics were bought from Shanghai Adamas Reagent Co., Ltd. (http://www.adamas-beta.com). The KMC aptamer DNA [29] (5′-NH2-TGGGGGTTGAGGCTAAGCCGA-3′) and its complementary single-stranded DNA (cDNA, 3′-TCGG CTTAGCCTCAACCCCCA-5′) were purchased from Songon Biotech Shanghai Co., Ltd. (http://www.life-biotech.com) and purified by HPLC. The milk sample was bought from a local supermarket.

Synthesis of signal probe (cDNA-conjugated AuNPs)

All glasswares for the experiments were utterly immersed overnight in aqua regia (HCl/HNO_3, 3/1 v/v) before use. The citrate reduction method has been applied to the synthesis AuNPs [24]. Concisely, 10 mL of trisodium citrate (1%) was quickly added to the boiling solution of 100 mL of hydrogen tetrachloroaurate (III) (1.0 mM) under vigorous and constant stirring for 15 min to award a wine-red solution. After that, the solution was cooled down gradually to the room temperature (RT) under continuous stirring and then stored in a refrigerator until use. The bioconjugation of AuNPs with cDNA was achieved by incubation 2 mL AuNPs with 25 μL of the cDNA (1 μM) under continuous stirring for 25 min in a dark environment at RT. The impurities were extracted by centrifuging the bioconjugates at 12000 rpm for 20 min. The precipitated cDNA@ Au bioconjugates were re-suspended in 2 mL PBS (pH 8.0) and kept at 4 °C until use. In such condition, the aptamer showed strong binding affinities to KMC with Kd lower than 100 nM (Fig. S1).

Fabrication of nanofibrous carrier (G-CA NFMs)

Typically, a homogeneous solution of 15 wt% CA in a solvent mixture of DMAc and acetone (1/2, wt/wt) was prepared. Electrospinning procedure was carried out using a syringe and a 19G needle with a flat tip at a voltage of 15 kV and a feeding rate of 1 mL h^{-1}. The CA NFMs were collected on an oilpaper sheet that was located 15 cm apart from the needle under a relative humidity of 30% and temperature of 28 °C. The residual solvents were removed by drying the NFMs in an oven at 200 °C for 1.5 h. The CA NFM thickness was controlled within 100 μm. Secondly, GA was grafted onto the CA NFMs using the alkaline reaction as depicted in Fig. S2. The grafting of the GA was achieved by direct reaction of the GA (2 g) with CA NFMs (0.5 g) by contact with ultrapure water (250 mL) under reflux for 96 h after the pH had been controlled to 9.5 ~ 10 (with a molar NaOH solution). The CA NFMs were then washed several times with ethanol and ultrapure water (until neutral pH) before being air-dried at RT for 24 h. The obtained grafted reaction between the GA and CA NFMs resulted in the formation of covalent bonds between amino groups of the GA and acetate groups of CA.

Preparation of test strips and experimented for KMC determination

To prepare the biosensor strips, the obtained G-CA NFM with a size of 1 cm × 1 cm was immersed and incubated in 50 mL of EDC/NHS solution for 1 h and dried at RT. The EDC/NHS solution was prepared by adding EDC (0.3 g) and NHS (0.2 g) to deionized water (50 mL). Then, the activated G-CA NFMs were incubated in 100 μL of aptamer (10 μM) in 5.0 mL of 50 mM MES buffer (pH = 5.5) at RT for 4 h. The unspecific adsorption was removed by rinsing with 5 mL of PBS for 3 times and the obtained aptamer-immobilized G-CA (AG-CA) NFMs were stored in PBS for further use.

Subsequently, the signal probes were assembled on the AG-CA NFMs by hybrid with the aptamer DNA [30, 31]. Briefly, the signal solution was dotting onto AG-CA NFMs several times (1 to 9 times). Each time, 10 μL of signal probes was dotted on (1 cm × 1 cm) AG-CA NFMs and air-dried at RT for 2 h. Then, the AG-CA NFMs assembled with signal probes were washed by 5 mL of PBS for 3 times and air-dried at RT for 2 h to acquire the biosensor strips with pink color.

Determination of KMC residues

The typical biosensing experiment of antibiotics was achieved as follows: antibiotics solutions (100 μL) of concentrations (2.5 ~ 80 nM) in PBS buffer were directly applied on colorimetric biosensor strips for 10 min at RT then washed by 5 mL of PBS and air-dried at RT for 20 min. The milk was pretreated to remove various proteins as shown in the Electronic Supporting Material (ESM).

Characterization

The characterization details were presented in the ESM.

Results and discussion

Design and principle of aptamer-based biosensor strips

The objective of the aptamer-based biosensor strips, consisting of signal probes (cDNA-conjugated AuNPs) and nanofibrous carriers, was shown in Scheme 1. While KMC was recruited as a model antibiotic to illustrate our strategy, firstly the signal probes were prepared by attaching of AuNPs covelantly to cDNA (a complementary single-stranded DNA of KMC aptamer). Moreover, a nanofibrous carrier for the signal probe was fabricated by electrospinning and modification. Generally, the nanofibrous carrier was designed based on three criteria. First, the solid nanofibrous carrier should have excellent hydrophilicity, large SSA, and high porosity. Second, specific chemical groups to interact with signal probes should be modified onto the NFM surface, which provided a large quantity active sites for assembling signal probes stably. Third, the disassembly of the signal probe from carrier can only trigger by KMC during the determination. The first criterion is fulfilled by choosing CA NFM as a primary platform, owing to their hierarchically multi-branching porous structure with large SSA [32]. To satisfy the last two requirements, our carrier design is based on DNA hybridization and aptamer-target complex interaction. Because the GA-grafted CA NFMs with plenty of carboxyl groups on the surface, it can be considered a suitable platform to label aptamer with amino groups [26]. Moreover, since the cDNA is the complementary DNA of aptamer, the signal probes constructed with cDNA and AuNPs were spontaneously hybridized with aptamer on the G-CA NFMs. In this case, signal probes are successfully assembled on the surface of the nanofibrous carrier, which would appear pink in color. During the KMC determination, the aptamer will preferentially bind with the added analyte via strong affinity effects (for example, hydrogen bonding, electrostatic forces, and spatial matching). Because the aptamer has a higher affinity to KMC than to its complementary DNA, the KMC can replace the signal probes then KMC-aptamer complex would be formed. Finally, the signal probes are released from carrier to the solution

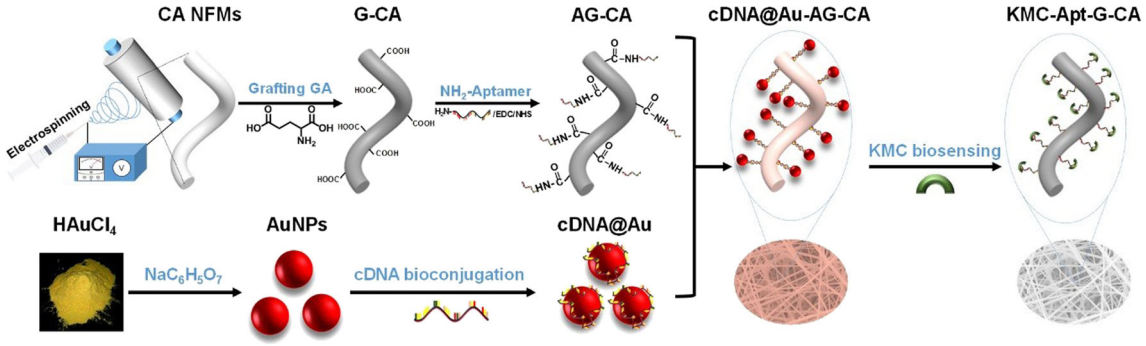

Scheme 1 Schematic illustration of the fabrication of CA, G-CA, and AG-CA NFMs, synthesis of AuNPs and their bioconjugation with cDNA, assembly of cDNA@Au onto the surface of the NFMs, and KMC biosensing process

media and the color of biosensor strips changes from pink to white.

Synthesis and characterization of cDNA@Au signal probes

As illustrated in Fig. 1a, the AuNPs showed typical extinction spectra for such particles with a maximum located at 517 nm due to the excitation of plasmons. For citrate-protected AuNPs, NP usually carries inter-particle electrostatic repulsion due to the preexisting citrate groups on the surface. After the bioconjugation process, the extinction maximum slightly shifted to around 525 nm as shown in Fig. 1a, and this phenomenon revealed that the cDNA-coated AuNPs were successfully formed [33]. cDNA with 21 bases in length was incubated with unmodified AuNPs, and van der Waals attraction between cDNA and AuNPs is strong compared with the repulsion between cDNA and negatively charged AuNPs. Therefore, the cDNA can adsorb on AuNPs gradually. It is worthy to mention that there is no observed color change after the bioconjugation process, as can be seen from Fig. 1d. AuNPs and cDNA@Au suspension were further investigated using TEM. The corresponding TEM images of AuNPs and cDNA@Au suspension were displayed in Fig. 1b and c. Both bare and conjugated Au NPs showed monodisperse and spherical morphologies, with a size range between 15 and 20 nm. Compared with AuNPs, a thin halo layer was observed around cDNA@Au, which was the signal of successful cDNA adsorption on the surface of the AuNPs. Evidence for the bioconjugation of the AuNPs with cDNA also came from Fig. S3. The addition of NaCl (50 mM) led to the aggregation of AuNPs, while there is no aggregation in the case of cDNA@Au. Increasing the ionic strength of the AuNPs led to disrupting the charge balance between the NPs. Consequently, the addition of enough salt can screen the repulsion between the NPs, leading to salt-induced aggregation. Nevertheless, cDNA is a random coil structure that adsorbs significantly to the AuNPs thus helping to stabilize the AuNPs at high salt concentration [34]. Moreover, the particle size distributions of AuNPs and cDNA@Au were measured by

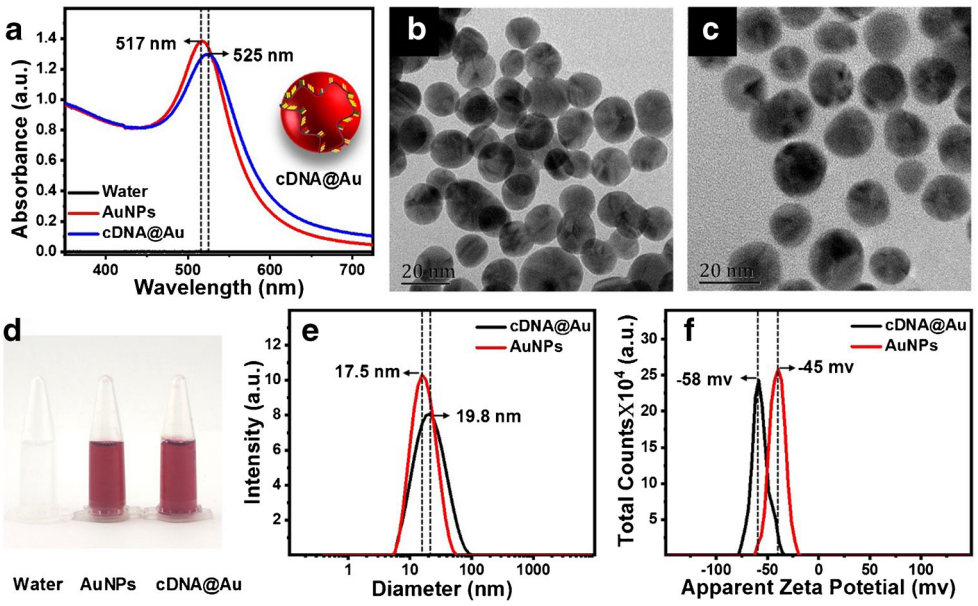

Fig. 1 **a** Ultraviolet-visible (UV-Vis) absorption spectra of water, AuNPs, and cDNA@Au. TEM images of **b** AuNPs and **c** cDNA@Au. **d** The photographic images of water, AuNPs, and cDNA@Au. **e** Dynamic light scattering (DSL) and **f** zeta potential of AuNPs and cDNA@Au

DLS. As shown in Fig. 1e, both samples showed a narrow diameter distribution; these results revealed that no aggregation occurred during the synthesis and bioconjugation processes. The average hydrodynamic radius estimated from DLS measurements was changed from 17.5 to 19.8 nm. Additionally, the surface zeta potential was changed from about − 45 mV to about − 58 mV, indicating that large amounts of negatively charged nucleic acid have stranded onto the surface of AuNPs (see Fig. 1f) [35].

Construction of the nanofibrous carrier

Endeavoring to offer a NFM-based carrier for signal probes assembling with some specific chemical bonds, GA was firstly grafted onto CA NFMs. The morphological behavior of CA and G-CA NFMs have been compared by FE-SEM as depicted in Fig. 2a and b. After the grafting process, fiber swelling phenomenon can be observed in the G-CA sample, yielding to a nanofiber diameter increasing as shown in Fig. S4a and b (more details were presented in the ESM). The FE-SEM results indicated that no deformation had been observed on the structure of NFMs after the modification process. Notably, as presented in corresponding contact angle images inserted in Fig. 2a and b, the wettability of CA NFMs (WCA = 125°) shifted to superhydrophilic after the GA modification.

The confirmation of the CA NFM modification through amide bond also came from FTIR spectral analysis. FTIR spectra of a GA, CA, and G-CA NFMs are presented in Fig. 2c (more details were presented in the ESM). The results suggested the covalent attachment of GA to the surface of CA NFMs through the formation of an amide bond, which was in good accord with the chemical structures of CA and GA. Thus, we derive that the GA-grafted CA NFMs with large SSA and the carboxylic acid groups have been fabricated successfully.

Furthermore, the TGA curves of GA, CA, and G-CA are presented in Fig. 2d. These results demonstrated that the CA have less water absorbability than G-CA. This phenomenon was an indication of the grafting of polar groups on the surface of CA NFMs [36]. To further verify the successful grafting of GA on CA NFMs, XPS was also applied to characterize the surface of the CA and G-CA NFMs. As seen in the XPS spectrum of the CA and G-CA, NFMs are presented in the inset in Fig. 2e. Just C1s and O1s bands appeared in the case of CA NFMs, while, a new band at binding energies of about 399.6 eV for N1s was observed in the spectrum of the G-CA NFMs, which can be attributed to amide groups. [37]. Consequently, the FE-SEM images and the ATR-FTIR spectra simultaneously with the TGA and the XPS spectra prove that GA has been grafted successfully onto CA NFMs with through the amide bond.

Since the performance of colorimetric recognition strongly relies on SSA [38], the SSA of the CA NFMs before and after the grafting process was examined through the N_2 adsorption–desorption technique. As seen in Fig. 2f, both curves represented type IV isotherm hysteresis based on the International Union of Pure and Applied Chemistry (IUPAC) classification. Besides, the tight H3 hysteresis loop demonstrates that the mesopores are unlocked; therefore, there is no considerable

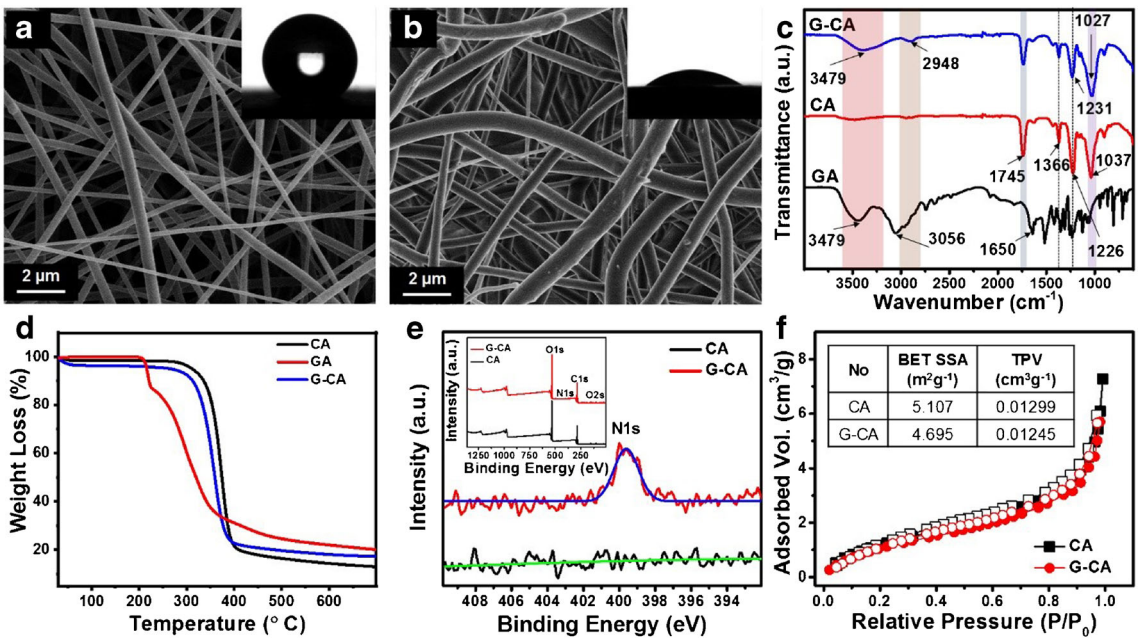

Fig. 2 Representative FE-SEM images of **a** CA NFMs and **b** G-CA NFMs. **c** FTIR spectra and **d** TGA patterns of GA, CA NFMs, and G-CA NFMs. **e** N 1s spectra of CA and G-CA NFMs and the corresponding XPS survey spectra are shown as inserts. **f** The nitrogen adsorption–desorption isotherms of CA and G-CA NFMs

interruption in-between capillary evaporation and N_2 condensation. BET SSA of G-CA NFM decreases slightly after chemical treatment due to the increase of the fiber diameter and surface roughness. This increase in fiber diameter represents a significant role in decreasing the SSA [39].

In order to construct a nanofibrous carrier for signal probe assembling, aptamer was immobilized on G-CA (AG-CA) NFMs for cDNA in signal probe hybridization. To confirm the desired structure, FE-SEM and XPS were employed to characterize the nanofibrous carrier. As shown in Fig. S5a, the feature of nanofibrous structure varied in the AG-CA NFM, and wrinkled fiber surfaces and a slight increase in average diameter were observed. Moreover, the evidence of successful aptamer immobilization was provided in XPS spectra (Fig. S6) (more details were presented in the ESM). Here, the results proved that aptamer has been well immobilized through the reaction between the COOH group on the G-CA NFMs and the NH_2 group of the aptamers and formation of CONH. The results meant that the AG-CA NFM acts as a carrier for signal probe assembling.

Characterization of signal probe assembled nanofibrous carrier

To verify whether the signal probe hybridization with the aptamers on the nanofibrous carrier surface can be established, a representative sample is prepared by incubating nanofibrous carrier with excessive signal probes to ensure the full combination. It can be clearly seen from the photograph of the representative sample that assembly process has produced an obvious color change from white to pink (Fig. S4b). In addition, after assembling, the monodisperse signal probes were well distributed on AG-CA NFMs without an obvious change in the particle size and shape as shown in the corresponding FE-SEM image (Fig. S5b). The aforementioned facts prove that the signal probes can be assembled on the nanofibrous carrier successfully.

To optimize the assembling amount of signal probes, different spotting time were designed. The assembling amount of signal probes onto the AG-CA NFMs was multiplying with the spotting time's increases as can be seen from the UV-vis spectra in Fig. S7a. The absorption peak of probe-assembled AG-CA NFMs was located at 510 nm. Noteworthy, the intensity of the signal probe-assembled AG-CA NFMs was also increasing as the spotting time is prolonging. However, RGB analysis data showed GRB sum reached a relatively stable region after 7 times (Fig. S7b). Therefore, spotting signal probes onto G-CA NFMs for 7 times were utilized as the optimal spotting time to prepare our biosensor strips, which is presented in pink color as shown in Fig. S7c.

Before our biosensor strips brought into use, EDX was used to study the surface chemical compositions of biosensor strips and verify their possibility to recognize KMC. The EDX spectra showed that C, N, and O were the main elements of the G-CA NFMs as represented in Fig. S8. Besides that, the weight ratio and EDX mapping of the corresponding elements were also inserted in Fig. S8. Noteworthy, Au element band has indeed existed in the EDX spectrum after spotting of signal probes, which is indicating assembly of cDNA@Au successfully on the NFMs again. After our strips reacted with KMC (60 nM, for 10 min), the pink color vanished. As shown in Fig. S5c, no particle-shaped structures can be observed on the carrier, which was in accordance with the color change, and this is in the light of the fact due to the leaching out of AuNPs. As displayed in Fig. S8, after KMC recognition, the weight of Au element is also decreased, which harmonize with the FE-SEM results reminded above (Fig. S5).

Additionally, the stability of signal probes on the biosensor strips was also checked by soaking the strips in the PBS buffer under continuous stirring at room temperature. They were taken out and used to detect KMC after 2, 5, 7, 15, 30, 60,

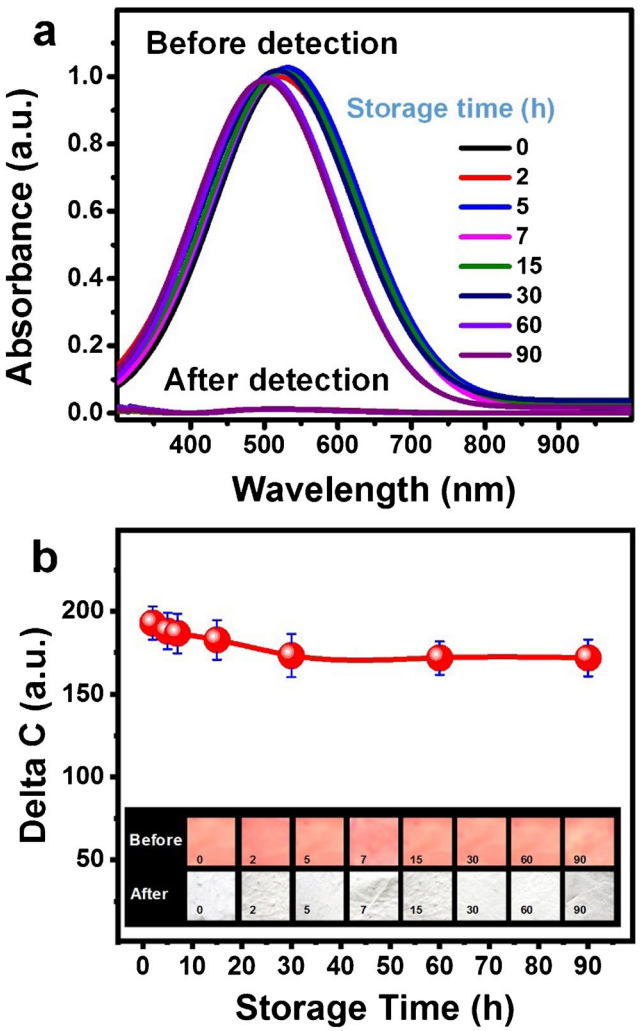

Fig. 3 **a** UV–vis absorption spectra. **b** ΔC obtained from RGB values of the colorimetric strips after soaking in the PBS of various storage time then used to detect KMC. Insets show the corresponding optical images

and 90 h. As exhibited in Fig. 3a, the biosensor strip color does not change after 90 h immersion. Here, the results indicating signal probes were stably and firmly assembled on the surface of the nanofibrous carrier. Likewise, as presented in Fig. 3b, the detectability of the biosensor strips displayed that no significant change in the C value occurs after soaking the strips in PBS for 90 h (the decrease of the C value was within 2.39–10.9%). Besides, the storage lifetime of the colorimetric biosensor was also checked by soaking the packed samples for half year. As can be seen from Fig. S9, no significant change in the C value occurs after soaking the packed samples for half year (the decrease of the C value was within 1.5–11.5%). Here, the results indicating our strips showed satisfactory storability without losing their detectability.

Sensing performance of biosensor strips

The sensing performance of the strips was evaluated upon exposure of the strips to different concentrations of KMC and incubation for 10 min at RT. As can be seen in Fig. 4a, due to rising of KMC concentration from 2.5 to 80 nM, the absorbance intensities of the biosensor strips at 510 nm decreased progressively, indicating an increase of AuNPs detaching rate owing to the effect of KMC as an accelerated agent. In addition, comparison color difference (C) values achieved from RGB values of the biosensor strips before and after determination of KMC demonstrated a perfect linear relationship with the KMC concentration ranging from 2.5 to 80 nM ($y = 4.073x+71.345$) ($R^2 = 0.995$). Figure 4c offers photographs of the biosensor strips after recognition of different KMC concentrations. Notably, the pink gradually vanished to white lightened with an increase in KMC concentration. However, the color changes of the biosensor strips even at 2.5 nM of KMC were still visually evident. For improving visual detectable of the biosensor strips, the color change was quantitatively evaluated by using RGB data. Figure 4b shows the ΔSUM values of the biosensor strips before and after exposure to different KMC concentrations. Noteworthy, the biosensor strips had detectability of concentration lower than 2.5 nM of KMC. Figure 4b displays also ΔR, ΔG, and ΔB values of the biosensor strips before and after exposure to different KMC concentrations. Worthwhile that a ΔG was the most pronounced, while ΔR is rarely altered, which is probably due to pink–white color transformation. Besides, the biosensor strips exhibited a remarkable sensitivity toward KMC compared with aptamers studied in earlier published reports for colorimetric recognition (Table S1). Here, the results referenced that visual recognition can be applying, which has various features such as high-sensitive, fast, easy to use, and relatively cheap for KMC recognition.

Moreover, the biosensor strips were exposed to different antibiotics including azithromycin (AZM), Chloramphenicol (CAM), cephalexin (CEF), Gentamicin (GEN), KMC, neomycin (NMC), norfloxacin (NRFX), oxytetracycline (OTC), Penicillin G (PC-G), and Sulfadiazine (SDZ) to study the selectivity property. As presented in Fig. S10, no color changes existed, which indicates that our colorimetric biosensor strip shows superior selectivity toward KMC.

Furthermore, the biosensor strips were applied for real samples including drinking water and milk by spiking them with various KMC concentrations. Subsequently, the biosensor strips, as well as ICP-AES, have determined the concentrations. Noteworthy, our results are in perfect congruence with results achieved by ICP-AES. Further, the average recoveries that we got are in the range of 98.608 ~ 103.224% for drinking water and 98.904 ~ 102.25% for milk, while the relative standard derivations found are between 1.061 ~ 1.37% for drinking water and 1.014 ~ 1.755% for milk (Table S2). This results demonstrated that the fabricated biosensor strips have good sensitivity to determine KMC from drinking water and milk,

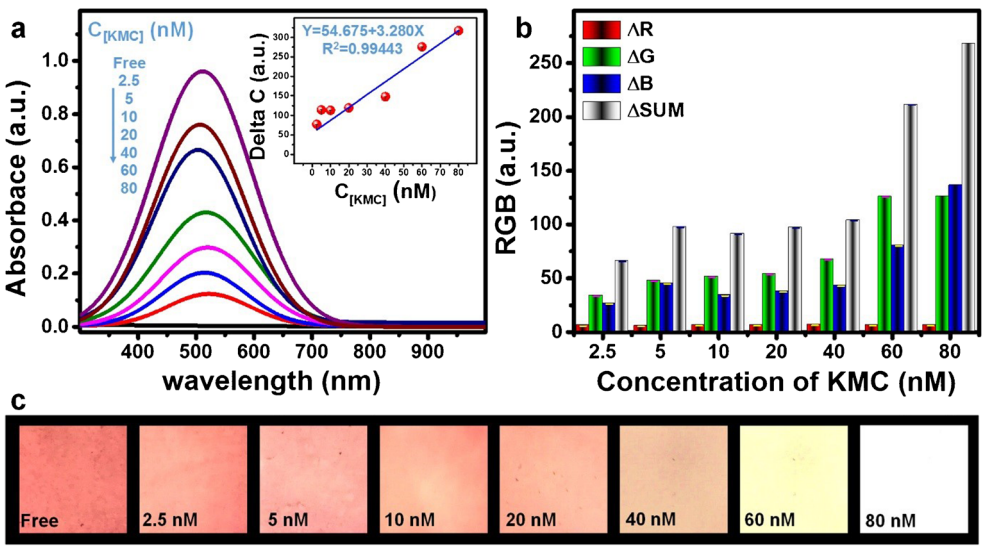

Fig. 4 **a** UV–vis absorption spectra, **b** RGB color change, and **c** optical images of the colorimetric strips after incubated in optimized leaching liquor added with various concentrations of KMC for 10 min. Inset of **a** the linear curve between ΔC obtained from RGB values of the strip before and after determination of KMC and concentration

which will have promising applicability for determination of KMC in real samples. However, the preparation process of the colorimetric biosensor strip is very long. Moreover, such biosensors can be applied as a useful screening tool to determine the antibiotics, if they have been commercially available.

Conclusions

We have successfully presented a novel strategy for optical biosensing of KMC. For the first time, nanofibers were decorated with aptamers with portability and stability. cDNA@Au, as the colorimetric agent, was stably assembled on the surface of aptamer-immobilized GA-grafted CA NFMs via DNA-DNA hybridization. Benefit from the excellent affinity of the aptamer to KMC, the signal probes immediately disassembled from the carrier when test strips interact with the target. As a result, the designed biosensor strips effectively combined the advantageous features of electrospun NFMs, AuNPs, and high specificity of aptamers that eventually produced a low detection limit, which can visually observe the resultant color change. Moreover, this method exhibited excellent selectivity and applicability to determine KMC in drinking water and milk.

Funding information This work was financially supported by the National Natural Science Foundation of China (51603034); the Fundamental Research Funds for the Central Universities (2232017D-03); the Seed Project of Key Laboratory of Textile Science and Technology of Ministry of Education (KLTST201622); and the 111 Project "Biomedical Textile Materials Science and Technology" (B07024).

Compliance with ethical standards

Conflict of interest The authors declare that they have no conflict of interest.

References

1. Tacconelli E, Pezzani MD (2019) Public health burden of antimicrobial resistance in Europe. Lancet Infect Dis 19(1):4–6
2. Gasser M, Zingg W, Cassini A, Kronenberg A (2019) Attributable deaths and disability-adjusted life-years caused by infections with antibiotic-resistant bacteria in Switzerland. Lancet Infect Dis 19(1): 17–18
3. Tagliabue A, Rappuoli R (2018) Changing priorities in vaccinology: antibiotic resistance moving to the top. Front Immunol 9:9
4. Shi D, Mi G, Wang M, Webster TJ (2019) In vitro and ex vivo systems at the forefront of infection modeling and drug discovery. Biomaterials 198:228–249
5. Wang S, Zeng X, Yang Q, Qiao S (2016) Antimicrobial peptides as potential alternatives to antibiotics in food animal industry. Int J Mol Sci 17(5)
6. Preu M, Guyot D, Petz M (1998) Development of a gas chromatography mass spectrometry method for the analysis of aminoglycoside antibiotics using experimental design for the optimisation of the derivatisation reactions. J Chromatogr A 818(1):95–108
7. Loffler D, Ternes TA (2003) Analytical method for the determination of the aminoglycoside gentamicin in hospital wastewater via liquid chromatography electrospray-tandem mass spectrometry. J Chromatogr A 1000(1–2):583–588
8. Gambardella P, Punziano R, Gionti M, Guadalupi C, Mancini G, Mangia A (1985) Quantitative-determination and separation of analogs of aminoglycoside antibiotics by high-performance liquid-chromatography. J Chromatogr 348(1):229–240
9. Arsand JB, Jank L, Martins MT, Hoff RB, Barreto F, Pizzolato TM, Sirtori C (2016) Determination of aminoglycoside residues in milk and muscle based on a simple and fast extraction procedure followed by liquid chromatography coupled to tandem mass spectrometry and time of flight mass spectrometry. Talanta 154:38–45
10. Hong F, Chen X, Cao Y, Dong Y, Wu D, Hu F, Gan N (2018) Enzyme- and label-free electrochemical aptasensor for kanamycin detection based on double stir bar-assisted toehold-mediated strand displacement reaction for dual-signal amplification. Biosens Bioelectron 112:202–208
11. Lan LY, Yao Y, Ping JF, Ying YB (2017) Recent progress in nanomaterial-based optical aptamer assay for the detection of food chemical contaminants. ACS Appl Mater Interfaces 9(28):23287–23301
12. Lin B, Yu Y, Cao Y, Guo M, Zhu D, Dai J, Zheng M (2018) Point-of-care testing for streptomycin based on aptamer recognizing and digital image colorimetry by smartphone. Biosens Bioelectron 100: 482–489
13. Shah K, Maghsoudlou P (2016) Enzyme-linked immunosorbent assay (ELISA): the basics. Br J Hosp Med 77(7):C98–C101
14. Li Y, Wang L, Wen Y, Ding B, Sun G, Ke T, Chen J, Yu J (2015) Constitution of a visual detection system for lead(ii) on polydiacetylene-glycine embedded nanofibrous membranes. J Mater Chem A Mater 3(18):9722–9730
15. Ma X, Li H, Qiao S, Huang C, Liu Q, Shen X, Geng Y, Xu W, Sun C (2020) A simple and rapid sensing strategy based on structure-switching signaling aptamers for the sensitive detection of chloramphenicol. Food Chem 302:125359
16. Zhang R, Wang Y, Qu X, Li S, Zhao Y, Zhang F, Liu S, Huang J, Yu J (2019) A label-free electrochemical platform for the detection of antibiotics based on cascade enzymatic amplification coupled with a split G-quadruplex DNAzyme. Analyst 144(16):4995–5002
17. Zhang K, Gan N, Shen Z, Cao J, Hu F, Li T (2019) Microchip electrophoresis based aptasensor for multiplexed detection of antibiotics in foods via a stir-bar assisted multi-arm junctions recycling for signal amplification. Biosens Bioelectron 130:139–146
18. Yi H, Yan Z, Wang L, Zhou X, Yan R, Zhang D, Shen G, Zhou S (2019) Fluorometric determination for ofloxacin by using an aptamer and SYBR Green I. Mikrochim Acta 186(10):668–668
19. Zhang K, Cao J, Wu Y, Hu F, Li T, Wang Y, Gan N (2019) A fluorometric aptamer method for kanamycin by applying a dual amplification strategy and using double Y-shaped DNA probes on a gold bar and on magnetite nanoparticles. Microchim Acta 186(2): 120
20. Wu Y-Y, Huang P, Wu F-Y (2019) A label-free colorimetric aptasensor based on controllable aggregation of AuNPs for the detection of multiplex antibiotics. Food Chem 304:125377–125377
21. Abedalwafa MA, Li Y, Ni C, Wang L (2019) Colorimetric sensor arrays for the detection and identification of antibiotics. Anal Methods 11(22):2836–2854
22. Ma Q, Wang Y, Jia J, Xiang Y (2018) Colorimetric aptasensors for determination of tobramycin in milk and chicken eggs based on DNA and gold nanoparticles. Food Chem 249:98–103

23. Xu C, Ying Y, Ping J (2019) Colorimetric aggregation assay for kanamycin using gold nanoparticles modified with hairpin DNA probes and hybridization chain reaction-assisted amplification. Microchim Acta 186(7):448
24. Abedalwafa MA, Li Y, Li D, Sanbhal N, Yang J, Wang L (2018) Aminated polyacrylonitrile nanofibers with immobilized gold-silver core-shell nanoparticles for use in a colorimetric test strip for copper(II). Microchim Acta 185(9):402
25. Reinholt S, Sonnenfeldt A, Naik A, Frey M, Baeumner A (2014) Developing new materials for paper-based diagnostics using electrospun nanofibers. Anal Bioanal Chem 406(14):3297–3304
26. Hui N, Sun X, Niu S, Luo X (2017) PEGylated polyaniline nanofibers: antifouling and conducting biomaterial for electrochemical DNA sensing. ACS Appl Mater Interfaces 9(3):2914–2923
27. Wang T, Zhang Y, Wang Y, Wei J, Zhou M, Zhang Z, Chen Q (2018) One-step electrospinning method to prepare gold decorated on TiO_2 nanofibers with enhanced photocatalytic activity. J Nanosci Nanotechnol 18(5):3176–3184
28. Li FL, Wang XY, Sun X, Guo YM (2018) Multiplex electrochemical aptasensor for detecting multiple antibiotics residues based on carbon fiber and mesoporous carbon-gold nanoparticles. Sensors Actuators B Chem 265:217–226
29. Song K-M, Cho M, Jo H, Min K, Jeon SH, Kim T, Han MS, Ku JK, Ban C (2011) Gold nanoparticle-based colorimetric detection of kanamycin using a DNA aptamer. Anal Biochem 415(2):175–181
30. Li N, Larson T, Nguyen HH, Sokolov KV, Ellington AD (2010) Directed evolution of gold nanoparticle delivery to cells. Chem Commun 46(3):392–394
31. Zhou J, Rossi JJ (2014) Cell-type-specific, aptamer-functionalized agents for targeted disease therapy. Mol Ther-Nucleic Acids 3:e169
32. Hu L, Yan X-W, Li Q, Zhang X-J, Shan D (2017) Br-PADAP embedded in cellulose acetate electrospun nanofibers: colorimetric sensor strips for visual uranyl recognition. J Hazard Mater 329: 205–210
33. Li F, Li J, Tang Y, Wang C, Li XF, Le XC (2016) Targeted enlargement of aptamer functionalized gold nanoparticles for quantitative protein analysis. Proteomes 5(1):1
34. Li H, Rothberg LJ (2004) DNA sequence detection using selective fluorescence quenching of tagged oligonucleotide probes by gold nanoparticles. Anal Chem 76(18):5414–5417
35. Xia Y, Liu M, Wang L, Yan A, He W, Chen M, Lan J, Xu J, Guan L, Chen J (2017) A visible and colorimetric aptasensor based on DNA-capped single-walled carbon nanotubes for detection of exosomes. Biosens Bioelectron 92:8–15
36. Wang H, Wen X, Zhang X, Liu C (2017) Acetylation of microcrystalline cellulose by transesterification in amimCl/DMSO cosolvent system. Molecules 22(9):1419
37. Celebioglu A, Demirci S, Uyar T (2014) Cyclodextrin-grafted electrospun cellulose acetate nanofibers via "Click" reaction for removal of phenanthrene. Appl Surf Sci 305:581–588
38. Abedalwafa MA, Li Y, Ni C, Yang G, Wang L (2019) Non-enzymatic colorimetric sensor strip based on melamine-functionalized gold nanoparticles assembled on polyamide nanofiber membranes for the detection of metronidazole. Anal Methods 11(29):3706–3713
39. Ma J, Wang X, Fu Q, Si Y, Yu J, Ding B (2015) Highly carbonylated cellulose nanofibrous membranes utilizing maleic anhydride grafting for efficient lysozyme adsorption. ACS Appl Mater Interfaces 7(28):15658–15666